1-1-2010

Response of 20 laterally loaded piles in sand

Wei-Dong Guo
Griffith University, wdguo@uow.edu.au

Bi Tang Zhu
Griffith University

Response of 20 laterally loaded piles in sand

Abstract

Closed-form solutions and their associated spreadsheet program (GASLFP) were developed by the first author for laterally loaded free- head piles in elastic-plastic media. The solutions show behaviour of a laterally loaded pile is dominated by net limiting force per unit length (LFP) fully mobilised along the pile to a depth called slip depth. They are characterised by three parameters of Ng, α o and n (to describe the LFP) and the soil shear modulus (Gs). Conversely, these parameters may be deduced by matching the predicted with measured response. To facilitate practical design, in this paper, the input values of Ng, α o, n and Gs were deduced in light of measured response of 20 piles tested in sand. The result allows effect of pile types, installation action, and dry or submerged sand to be clarified. In addition, using analogy to pipeline-soil interaction, a new alternative expression described by the parameters kp, α o and n is proposed to construct the LFP. The use of the previous parameter Ng and the new kp is discussed at length. Critical responses for typical deflection levels have also been provided. This back-analysis is elaborated via three typical cases.

Keywords

piles, 20, sand, response, loaded, laterally

Disciplines

Engineering | Science and Technology Studies

Publication Details

Guo, W. & Zhu, B. (2010). Response of 20 laterally loaded piles in sand. Australian Geomechanics Journal, 45 (2), 67-84.

Date revised: 26 May 2010

Title: Nonlinear Response of 20 Laterally Loaded Piles in Sand

Authors: Wei Dong Guo[1] and Bi Tang Zhu[2]

Affiliation and address:

[1]Wei Dong Guo

Corresponding author
School of Engineering, Griffith University, Gold Coast Campus
PMB 50, Gold Coast Mail Centre, QLD, 9726
Tel: 617-5552 8803
Fax: 617-5552 8065
Email: **w.guo@Griffith.edu.au**

[2]Bi Tang Zhu
School of Engineering, Griffith University, Gold Coast Campus
Currently, Arup Pty Ltd, Level 4 108 Wickham Street, Fortitude Valley, Qld, 4006

Number of words: 7576
Number of tables: 3
Number of figures: 18

Nonlinear response of 20 laterally loaded Piles in Sand

Wei Dong Guo, and Bi Tang Zhu

School of Engineering, Griffith University, QLD, Australia

Summary: Closed-form solutions and their associated spreadsheet program (GASLFP) were developed by the first author for laterally loaded free- head piles in elastic-plastic media. The solutions show behaviour of a laterally loaded pile is dominated by net limiting force per unit length (LFP) fully mobilised along the pile to a depth called slip depth. They are characterised by three parameters of N_g, α_o and n (to describe the LFP) and the soil shear modulus (G_s). Conversely, these parameters may be deduced by matching the predicted with measured response.

To facilitate practical design, in this paper, the input values of N_g, α_o, n and G_s were deduced in light of measured response of 20 piles tested in sand. The result allows effect of pile types, installation action, and dry or submerged sand to be clarified. In addition, using analogy to pipeline-soil interaction, a new alternative expression described by the parameters k_p, α_o and n is proposed to construct the LFP. The use of the previous parameter N_g and the new k_p is discussed at length. Critical responses for typical deflection levels have also been provided. This back-analysis is elaborated via three typical cases.

Key words: piles, limiting force profile, non-linear response, lateral loading, soil-structure interaction

1 INTRODUCTION

Numerical approaches capitalised on p-y concept have been widely used to investigate the behaviour of laterally piles in sand (Reese et al. 1974; FHWA 1993). Their accuracy predominantly relies on simulating the development of the limiting force mobilized between the pile and soil from groundline (Randolph et al. 1988; Guo 2001; Guo 2006). The distribution profile of limiting force per unit length (LFP) along the pile is currently ascertained using

empirical or semi-empirical methods (Broms 1964; Reese et al. 1974; Barton 1982). These methods work well in relevant cases, but they do not always provide good prediction. Perhaps these methods are normally capitalised on soil failure mode only (Guo 2006), which cannot cater for well the impact of the following: Pile-soil relative stiffness, pile size, types of piles, installation procedure, sand dilatancy, sand non-homogeneity, presence of free water, and so forth. Note that the impact of pile-head conditions, and pile-pile interaction may be well accommodated using theoretical solutions (Guo 2009).

Elastic-plastic, closed-form (CF) solutions were developed for laterally loaded free-head piles (Guo 2001). The solutions were implemented into a spreadsheet program called GASLFP (Guo 2001; Guo 2006) operating in EXCEL^{TM}, with nonlinear calculation being executed via purposely designed macros. Predictions about quite a large number of piles were made previously, from which the following salient features are noted (Guo 2001; Guo 2006):

1. Response of a laterally loaded pile is primarily dominated by limiting force profile and the pile-soil relative slip depth to which the force (resistance) is fully mobilised.
2. Responses of deflection, slope, bending moment, shear force and soil resistance under any load levels may be uniquely predicted using a given LFP and soil modulus.
3. The LFP is sufficiently accurately described by 3 parameters, regardless of stress (load) levels; and it can be constructed using six different methods.
4. The LFP and the maximum mobilised slip depth may be deduced in terms of measured nonlinear response of piles, which should cater for the integral effect of the main influence factors.

To facilitate use of the closed-form solutions, back-estimation of LFP has been carried out since 2003. Against measured data and in light of the GASLFP, over seventy free-head, single piles have been analysed so far, embedded in clay, sand, or rock. The obtained shear modulus and LFP for 32 piles in clay were presented previously (Guo and Zhu 2005). In particular, limiting force mobilised along 18 out of 32 piles was found ~ 70% less than that gained using Matlock's method

(Matlock 1970), but it compares well with Hansen's suggestion (Hansen 1961). This paper presents the analysis conducted for 20 free-head piles embedded in sand, to calibrate methods of constructing LFP for piles in sand.

2 ELASTIC-PLASTIC THEORY

The current study on the LFP employs the closed form solutions developed previously (Guo 2001; Guo 2006). The theory, as recaptured herein is for a free-head, infinitely long pile that is schematically depicted in Figure 1(a). A lateral load P_t is applied on the pile at an eccentricity, e above mudline. The pile is free to rotate and translate with no constraints imposed at the head and along the effective pile length except for the soil resistance. The elastic pile has a deflection y at depth x (at the mudline, $x = 0$). The pile-soil interaction is simulated by a series of pairs of springs in series with sliders distributed along the pile shaft. The interaction among the springs in the lower elastic zone ($x \geq x_p$) is accounted for by using a coupled load transfer model (Guo and Lee 2001). The independent springs are linked by a fictitious membrane that has a constant tension, N_p, compared to negligible tension (thus $N_p = 0$) in the upper plastic zone ($x < x_p$). The main features for the model are as follows:

- The eccentric head-load (see Figure 1(a)) is replaced with the load P_t and a moment, M_t (= $P_t e$) exerted at the mudline, Figure 1(b).
- An idealized elastic-plastic p-y curve, as illustrated in Figure 1(c), is used for each spring-slide element, for which the gradient of the curve is the subgrade modulus, k of the spring; and the limiting force per unit length p_u sets the resistance threshold of the slider.
- The force per unit length p is stipulated to be fully mobilised from the mudline and extends to a depth called slip depth, x_p. Above the depth, the p is equal to p_u ($x \leq x_p$), otherwise with $x > x_p$, the p is proportional to the pile deflection.

2.1 Elastic state: Coupled load transfer model *(Guo and Lee 2001)*

The coupled model for elastic state is depicted in Figure 1(b) (for a depth being greater than x_p). The governing equation for the pile embedded in an equivalent, homogenous and isotropic medium was derived using variational approach as (Guo and Lee 2001)

$$\frac{d^2}{dz^2}\left(E_p I_p \frac{d^2 y}{dz^2}\right) - N_p \frac{d^2 y}{dz^2} + ky = 0 \qquad 0 \le z \le L - x_p \tag{1}$$

where z = x-x_p, i.e. z is measured from the slip depth; E_p = Young's modulus of an equivalent solid pile, $E_p = E_p I_p/(\pi d^4/64)$; $E_p I_p$ = flexural rigidity of the pile; k = modulus of subgrade reaction; N_p = fictitious tension that links the springs, and

$$k = \frac{3\pi G_s}{2}\left(2\gamma_p \frac{K_1(\gamma_p)}{K_0(\gamma_p)} - \gamma_p^2\left(\left(\frac{K_1(\gamma_p)}{K_0(\gamma_p)}\right)^2 - 1\right)\right) \qquad N_p = \frac{\pi d^2}{4} G_s \left(\left(\frac{K_1(\gamma_p)}{K_0(\gamma_p)}\right)^2 - 1\right) \tag{2}$$

where $K_i(\gamma_p)$ = modified Bessel function of second kind of i^{th} order (i = 0, 1); $\gamma_p = k_1(E_p/G^*)^{-0.25}$

d = outside diameter of the equivalent solid pile; L = pile embedment length; $G^* = (1 + 0.75\ \nu_s)\ G_s$, ν_s and G_s = Poisson's ratio and shear modulus of the soil, respectively; k_1 = 1.0 ~ 2.0, with the low and the high values for pure lateral loading and pure moment loading, respectively. Advantage in using Equation (2) compared to existing approaches was discussed at length by (Guo 2001). The solutions are developed for a pile having a length exceeding a critical length, L_c given by $L_c = 1.05d(E_p/G_s)^{0.25}$. Given $E_p/G_s = 10^2 \sim 10^5$, it follows $L_c = (3.3 \sim 18.7)d$. It is adequate to use an average shear modulus G_s over this critical depth, thus a recursive process for determining L_c is required. It is noted that an extra length beyond L_c will induce negligible influence on response of the pile; whereas a short pile with $L < L_c$ may render another slip to be developed from the pile tip (Guo 2004; Guo 2008).

2.2 Plastic state: Limiting force profile (LFP)

With respect to the upper, plastic zone ($0 \le x \le x_p$), limiting force profile (LFP) was encapsulated into a generic form (Guo 2001; Guo 2006) that follows

$$p_u = A_L(\alpha_o + x)^n \quad (3)$$

where p_u = limiting force per unit length [FL^{-1}]; $A_L = \gamma_s N_g d^{2-n}$, gradient of the LFP [$FL^{-1-n}$]; α_o = a constant to include the force at the mudline [L]; x = depth below the mudline [L]; n = power to the sum of α_o and x; N_g = limiting force factor with $N_g = s_g K_p^2$; $K_p = \tan^2(45^o + \phi_s/2)$, the passive earth pressure coefficient; s_g = an integral factor to cater for influence of all factors; and γ_s = effective unit weight of the soil [FL^{-3}]. A_L was taken as $\gamma_s N_g d$ ($N_g = K_p^2$, n = 1) for rigid piles (Guo 2003). The governing equation for the laterally loaded pile in the plastic zone is

$$\frac{d^2}{dx^2}\left(E_p I_p \frac{d^2 y}{dx^2}\right) = -A_L(x+\alpha_o)^n \qquad 0 \le x \le x_p \quad (4)$$

2.3 Elastic-plastic solutions

Equations (1) and (4) for the free-head pile (Figure 1) were solved simultaneously. The results are called elastic-plastic solutions, and are presented in compact, closed-form expressions by (Guo 2001; Guo 2006). As long as the pile has a length exceeding the sum of the critical length L_c and the maximum slip depth, x_p at any stage, the solutions are rigorously applicable. Note that the length L_c refers to the portion of pile length in elastic zone. The main features of the solutions were briefed previously in the '*introduction*'. Apart from the imposed loads P_t and M_t, they are primarily functions of the parameters detailed below:

- The reciprocal of the characteristic length of the pile λ ($=[k/(4E_pI_p)]^{0.25}$);
- The slip depth x_p, and the LFP (thus, the parameters N_g, α_o, and n).

These solutions were implemented into the spreadsheet program GASLFP (Guo 2001; Guo 2006), with which the calculations presented herein were undertaken.

3 BACK-ESTIMATION OF LFP

With development of pile-soil relative slip, the three parameters N_g, α_o, and n are uniquely deduced by matching three predicted responses with measured ones. The 'match' may include the relationships of load (P_t) versus maximum bending moment (M_{max}), load (P_t) versus mudline

displacement (y_o) or pile-head displacement ($y_t = y_o+\theta_o e$), and M_{max} versus depth of the M_{max} (x_{max}). Note θ_o (in radian) is the angle of pile-head rotation at ground level. They may also be based on the profiles of bending moment or deflection at a typical load with certain slip depth.

3.1 Parameters and procedure for current analysis using GASLFP

The procedure for investigating pile response using GASLFP was elaborated previously (Guo 2006). It is recaptured herein by focusing on piles in sand:

(1) Input the pile geometries of d, and L; flexural stiffness of E_pI_p, and I_p (to find the equivalent E_p); and the imposed load, P_t and its eccentricity, e.

(2) Compute an average soil shear modulus G_s over a depth of $14d$ (initially). This may be correlated with an average blow count of standard penetration test (*SPT*). Poisson's ratio may be assumed accordingly.

(3) Evaluate the critical pile length, L_c via iteration, and a new G_s over the length is estimated.

(4) Compute the k and the N_p using Equation (2).

(5) Determine the LFP using an average effective unit weight γ_s, and frictional angle of soil ϕ_s over a depth of $5d$, respectively, in simulating a pile deflection of ~ $0.2d$ at mudline.

(6) Estimate and input the parameters α_o, n and N_g, it is often appropriate to use n = 1.7, α_o = 0, and $N_g = (0.6\sim2.5)K_p^2$ with $K_p = \tan^2(45+\phi_s/2)$.

(7) The calculated effective depth is the sum of L_c and $10d$, which should be less than the pile length L, otherwise solutions for a rigid pile should be used (Guo 2003; Guo 2004).

Conversely, the parameters α_o, n and N_g may be deduced by best match with available measured response using the same steps.

An average value of initial modulus G_s should be used over an effective depth of L_c+$10d$. Dependent of L_c (thus load level), G_s is generally taken as a constant over the entire loading regime, so is the LFP (n, α_o, and N_g). The LFP thus deduced against measured data is referred to

as Guo LFP herein. It was also constructed using the previous suggestions (Hansen 1961; Broms 1964; Reese et al. 1974; Barton 1982), and is termed as respectively Barton LFP, Broms LFP, etc.

3.2 Justification of back-figured parameters

Finite element analysis on pipeline-soil interaction (Guo and Stolle 2005) shows the impact of sand dilatancy, pipeline scale (size), embedment depth, and stress hardening, etc. The analysis together with experimental data indicate that normalized limiting force along a pipeline, $p_u/(\gamma_s d^2)$ may be obtained using Equation (5).

$$\frac{p_u}{\gamma_s d^2} = \frac{\gamma}{\gamma_s}\left(\frac{x}{d}\right)^{1.35} \frac{k_p}{d^{n_p}} R_\psi \qquad (5)$$

where k_p = 3~6, n_p = 0.2~0.25, d = (pipeline) diameter in m, x = the burial depth measured between mudline and pipe center. $R_\psi = 1 + 0.23(1 + 0.24x/d)\sin(\psi)$, which is designed to capture the impact of soil dilation angle of ψ. The unit weight γ is normalised herein using effective unit weight γ_s.

Lateral pile-soil interaction is likely to be affected by the factors unveiled for the pipeline-soil interaction, namely sand dilatancy (Fan and Long 2005), the pile size, and embedment depth, etc, in addition to those factors mentioned previously. The limiting pressure mobilised on either a pipeline or a lateral pile was gained successfully using plasticity theory (Randolph and Houlsby 1984; Murff et al. 1989). A pipeline follows the same governing equation (4) for a lateral pile (Rajani and Morgenstern 1993). Thereby, Equation (5) is extended herein into lateral piles.

As the confinement stress increases with depth, the dilation angle should decrease. The R_ψ thus reduces from ground surface to pile base, and may be approximately proportional to $(x/d)^{-0.17}$. Thereby, the $p_u/(\gamma_s d^2)$ is proportional to $(x/d)^{1.18}$ in light of Equation (5), as the values of γ/γ_s and k_p/d^{n_p} are constant with depth. This power of 1.18 is rather close to 1.0 noted for rigid piles in sand (Broms 1964; Guo 2008). Consequently, the p_u on a pipeline and a lateral pile do show similar variation with depth for rigid short piles. This result is not the scope of current study.

The match between Equation (3) and (5) requires a linearly increasing ψ with depth (from zero at mudline to ϕ_s at pile base), which allows the R_ψ to be approximated by $(x/d)^{0.17}$. Equation (5) for pipelines thereby is transformed into Equation (6) for piles in sand.

$$\frac{p_u}{\gamma_s d^2} = \frac{\gamma}{\gamma_s}\left(\frac{x}{d}\right)^{1.52} \frac{k_p}{d^{n_p}} \tag{6}$$

Comparing Equation (6) with (5) indicates the normalised pressure p_u increases with a power of n = 1.52 after incorporating the impact of sand 'dilatancy'. The values of 'n = 1.52' fit well with those used for piles in sand (Guo 2009). Nevertheless, the dilatancy angle cannot render an increase R_ψ with depth but for some unknown factors, indicating the difference between a pipeline and a long pile.

A further comparison between Equation (6) and Equation (3), assuming n = 1.52, and α_o = 0 shows that

$$s_g = \frac{\gamma}{\gamma_s K_p^2} \frac{k_p}{d^{n_p}} \tag{7}$$

Equation (6) was used to fit the overall trend of the deduced LFP [Guo LFP, Equation (3)] within the maximum x_p. This allows the k_p to be gained (as shown in later examples). A compromise is used in the fit to make up the inconsistent n of 1.7 for piles (Guo 2006), and 1.35~1.52 for pipelines. It also yields different s_g using Equation (7) and the definition of N_g/K_p^2 in Equation (3). To avoid confusion, Equation (7) will be termed as s_g, and presented along with N_g/K_p^2 (see Table 2 for comparison). Limiting pressure mobilised on a laterally loaded pile (Randolph and Houlsby 1984) is about twice that mobilised along a pipe penetrated into cohesive soil (Murff et al. 1989). This analogy, if applicable to sand, indicates k_p = 6~12 for piles, which is discussed next.

4 THREE TYPCIAL CASE STUIDIES

4.1 Case I- (PS1) Open-ended Pipe Pile in Submerged Dense Sand

Cox et al (Cox et al. 1974) reported lateral loading tests on two open-ended steel pipe piles driven into a uniformly graded fine sand at Mustang, Texas. Each pile was 21 m long, 610 mm in outside diameter, and 9.53 mm in wall thickness. Each had a flexural stiffness E_pI_p of 163 MN-m^2, and moment of inertia I_p of 8.0845×10^{-4} m^4, which enable the equivalent E_p to be estimated as 24.0 GPa. Pile one test was conducted under static lateral load at an eccentricity e of 0.305 m above mudline. The following responses were measured, and are plotted in Figure 2 for the static pile test (referred to as PS1): Pile-head load (P_t) versus groundline deflection (y_o); Load (P_t) vs maximum bending moment (M_{max}) ; Load (P_t) vs groundline rotation in radian (θ_o); and bending moment distribution along the pile at a head-load of P_t = 210 kN.

The furthest surface (from the neutral axis) of the pile would first yield at a bending moment of 640 kN-m, and a fully plastic hinge would be formed at a moment of 828 kN-m (Reese and Van Impe 2001). Variation of bending stiffness after the first yield is negligible, and the pile may behave elastically prior to the formation of a hinge.

The sand had a friction angle ϕ_s of 33° in terms of a relative density D_r of 0.9 (Kulhawy and Mayne 1990). The submerged unit weight γ_s was 10.4 kN/m^3. During the test, the free water was maintained at about 150 mm deep. The average blow count of *SPT*, $\widetilde{N}$ (bar '~' denotes an average value over depth) was 18 over a depth of 10d (d = outside diameter). The pile (see Table 1) was investigated herein with the input parameters (see Table 2) that follows: ν_s = 0.3, α_o = 0 m, n = 1.7, G_s = 10.52 MPa or 0.58N (MPa), and $N_g = 0.93K_p^2$. The LFP is plotted in Figure 2(a).

The GASLFP allows a good simulation of the pile response compared to the measured data, as can be seen from Figure 2. Substituting the values of G_s and E_p into Equation (5), the critical length L_c was estimated as 4.43 m (≈ 7.3d). At the maximum imposed load P_t of 266.8 kN, the M_{max} was estimated as 494.4 kN-m (< M_u) and the slip depth x_p as 1.94m (3.18d). Thus, the total

effective length of 6.37 m (= $L_c + x_p$) calculated is far less than the pile embedment. The use of the GASLFP is legitimate.

Overall, the *LFP* profile (Guo *LFP*) over the maximum depth of x_p (= 3.18d) differs from the Reese *LFP* in shape, but the profiles offer similar total forces over the respective maximum slip depths. The overall agreement with measured data is slightly better using the current Guo *LFP*. The k_p was deduced as 6.5 (see Table 2) using Equation (6) to fit the Guo *LFP* within x_p = 3.18d. The low value of k_p reflects the combined impact of the submerged unit weight, the low displacement pipe pile, and the less compactable uniformly graded fine sand.

4.2 Case II – (PS2) Open-ended Pipe Pile in Medium Dense Sand

Brown et al. (Brown et al. 1988) reported tests on a large-scale group of steel piles and an isolated single pile subject to two-way cyclic lateral loading. The piles in the group were filled with concrete while the isolated pile was hollow. The single pile (referred to as PS2) was 13.115m long, 273 mm in outside diameter, and 9.27 mm in wall thickness with $I_p = 6.686\times10^{-5}$ m^4 and E_pI_p = 13.708 MN-m^2, respectively. Considering the reinforcing effect of concrete, the equivalent E_p was estimated as 5.03×10^4 MPa (= $13.708/\pi/0.273^4\times64$), assuming as a solid pile.

The subsoil around the single pile consisted of 2.9 m (about 10.6d) of medium dense sand that was underlain by very stiff clay. The sand had ϕ_s = 38.5°, γ = 15.4 kN/m^3, and $\tilde{N}$ = 35. The lateral loads were imposed approximately at e = 0.305 m above the ground line. The measured response of the pile for cycle 1 is plotted in Figure 3, showing deflection at load point y_t, maximum bending moment M_{max}, and distribution of bending moment with depth at P_t = 86.7kN.

A good prediction (see Figure 3) was made compared to the measured data using GASLFP and the following parameters: ν_s = 0.3, α_o = 0 m and n = 1.7, G_s = 16.5 MPa or 0.47 N (MPa), and $N_g = 0.66K_p^2$. The G_s and E_p allow the pile critical length L_{cr} to be computed as 2.13 m (≈7.8 d). The *LFP* is presented in Figure 3(a). The k_p was deduced as 13 using Equation (6) within x_p = 5.18d. The twice times higher k_p compared to the previous 6.5 seems to compatible with the

increase in blow counts of $\widetilde{N}$ (35 in this case, 18 in the previous case).

4.3 Case III - (PS3) Driven Pile in Two-Layered Soil

A single pile C was driven into a two-layered soil (ie. a sand layer that extended to a depth of 15.4 m from the ground level, which was underlain by a silt layer with a undrained shear strength s_u of 55 kPa). It was instrumented and tested to measure the bending strain along the pile length. The pile was 23.3 m in length, and 610mm in diameter, and had an E_pI_p of 166.04 MN-m^2. The blow count of *SPT*, *N* of the sand layer was reported as: 12 (in depth of 0 ~ 11.0 m), 8 (11.0 ~ 13.8 m), and 16 (13.8 ~ 15.4 m), respectively. Other properties are as follows: γ_s = 16.5 kN/m^3. G_s= 7.68 MPa, and ϕ_s = 28^o, respectively (deduced using $\overline{N}$ over a depth of 11 m). This allowed L_c and the effective length to be estimated as 7.9*d* and 17.9*d* (= L_c + 10*d*), respectively. The effective length located in the top layer, which rendered the problem to be simplified as a pile in a single layer. This pile was studied previously (Guo 2006), as recapitulated below.

Assuming n = 2.0, and α_o = 0, A_L was computed as 126.59 kPa/m. The *LFP* is then plotted as 'Guo (2006)' in Figure 4(a). The pile-head displacement and maximum moment were predicted and are illustrated in Figure 4(b) and (c), respectively. In comparison with the measured data, the displacement, and the depth of maximum bending moment were well predicted, but the bending moment (see Figure 4(b)) was slightly overestimated.

To elucidate the overestimation, a new back-estimation was attempted by matching with the measured curves of P_t~ y_o, and P_t ~M_{max} but not the curve of P_t ~x_{max} (the depth of the M_{max}). This fit is depicted in Figure 4 as 'GASLFP', which renders G_s = 3.23 MPa, ϕ_s = 35^o, and n = 1.7.

Compared to Guo (2006)'s back-estimation, the G_s reduces by 50%, and the n drops from 2.0 to 1.7. The use of ϕ_s = 35^o is to reflect the impact of driving action that leads to an increase in N_g by 77%. As seen in Figure 4(a), the limiting force per unit length p_u deduced increase by 3 times. The full resistance at a pile-head load of 443.2 kN was mobilized to a depth of 0.994 m (1.63d), compared to 1.9 m (3.1d) obtained in the previous analysis. The significant difference in

the LFP actually leads to slight difference in the total resistance over the respective slip depth. The prediction of load-displacement curve is insensitive to shape of the *LFP*, but the load-moment curve is to certain extent.

The k_p was deduced as 27 to fit the Guo *LFP* over x_p = 1.64d. This may occur owing to increase in SPT following driving action. This value should be smaller, as a stiffer than measured response is matched at high load levels. The k_p is 9, should the LFP of Guo (2006) be matched, which is more legitimate and on safe side.

5 ANALYSES OF 20 PILES

5.1 Analyses of 20 piles tested in sand

Response of 20 piles tested in-situ in sand was analyzed using the GASLFP. The properties of the piles and the sand are provided in Table 1, along with the loading eccentricities. The analysis allows the parameters of G_s, N_g, and k to be deduced, which are tabulated in Table 2. The Guo LFP is plotted in Figures 2-16 for each pile. It was subsequently fitted using Equation (6), which offered k_p. The k_p obtained in turn allows the s_g to be calculated using Equation (7). Both k_p and s_g are tabulated in Table 2. A good comparison between the predicted and the measured response for all but PS4 is noted in Figures 2-16, in which the critical responses at a mudline deflection y_o = 0.1d, or under a maximum imposed load (P_{max}) are also highlighted in the symbols ◑, and ■. Concerning y_o = 0.1d and 0.2d, provided in Table 3 are normalised pile-head load, $P_t/\gamma_s d^3$; normalised slip depth, x_p/d; slope at groundline, θ_o (%); normalised maximum bending moment, $M_{max}/\gamma_s d^4$; and normalised depth of maximum bending moment, $\boldsymbol{x_{max}/d}$.

The piles, loading eccentricities, and soil properties are summarized in Table 1.

(a) $E_pI_p = 8.6\times10^{-5}$ ~527.4 MN-m^2, with the majority E_pI_p = 20~70 MN-m^2, and E_p = (1.60~5.99) $\times10^4$ MPa

(b) d = 18.2 ~ 812.8 mm, and the majority d = 120 ~ 480 mm.

(c) e (eccentricity of the applied loads) = 0.01 ~ 2.2 m.

(d) ϕ_s = 29.6 ~ 43°, ranging from loose to dense sand;

(e) G_s = 0.3~0.45 MPa (model piles), 3.2~18.0 MPa (prototype piles), N = 10~35.

The input parameter k and those for determining LFP are provided in Table 2, which shows:

(a) G_s = (0.25~0.62)N (MPa) with $\overline{G}_s$ = 0.50N (MPa) (bar '-' denotes average value for all pertinent piles in this paper). In other words, Young's modulus E_s = (0.65~1.6)N (MPa), with $\overline{E}_s$ = 1.3N (MPa). This correlation is akin to those gained previously (Guo 2006), and agrees with E_s = (0.5~1.5)N (MPa) (Kulhawy and Mayne 1990), and E_s = (1.4 ~1.8)N (MPa) (Kishida and Nakai 1977).

(b) k = (2.38~3.73)G_s, with $\overline{k}$ = 3.23G, which is slightly lower than k = 4G_s deduced previously (Randolph et al. 1988).

(c) n = 1.7, α_o = 0, and N_g = (0.4~2.8)K_p^2 for all piles embedded in uniform soil profiles; and $\overline{N}_g$ = 1.29K_p^2.

(d) n > 1.7 for shear strength exhibiting more acute increases than linearly with depth such as around pile PS3, and vice versa.

(e) N_g = (0.4 ~1.0)K_p^2 with respect to the bored pile (PS14) or the open-ended pipe piles (PSs1~2, 7, 19~20). N_g = (1.1~2.5)K_p^2 for the driven pipe piles (PSs 3~4, 12~13, and 15~18). N_g = (1.6~1.8)K_p^2 for the reinforced pipe piles (PSs8, 10), and large sectional area pile (PS 11).

(f) Imposing a fixed-head condition, the gradient of the limiting resistance reduces to 25% that mobilized around a free-head pile (Guo 2005), as it is evident for the pile PSs 12 and 13 compared to PS 14.

Table 3 shows L_c was (6.7~15.9)d, with $\overline{L}_c$ = 9.5d. Other critical responses with respect to a ground-level displacement y_o of 0.1d are:

- Maximum x_p = (1.63 ~ 5.18)d, with $\overline{x}_p$ = 3.6d, and $\overline{L}_c + \overline{x}_p$ = 13d; x_{max} = (3.35 ~ 6.1)d, with $\overline{x}_{max}$ = 4.07d; θ_o = (1.45~2.95)%, with $\overline{\theta}_o$ = 2.17%; $P_t/\gamma_s d^3$ = 80~800 (see Figure 17), and $M_{max}/\gamma_s d^4$ = 250~4,000 (see Figure 18).

Furthermore, with respect to y_o =0.2d, it follows:

- Maximum x_p = (2.22~ 6.39)d, with $\bar{x}_p$ = 4.61d, and $\bar{L}_c + \bar{x}_p$ = 14d; x_{max} = (3.85 ~ 6.55)d, with $\bar{x}_{max}$ = 4.67d; θ_o = (2.85 ~ 5.41)% with $\bar{\theta}_o$ = 4.03%; $P_t/\gamma_s d^3$ =130~1,300 (see Figure 17) and $M_{max}/\gamma_s d^4$ = 460~6,550 (Figure 18).

Overall, Figures 2~16 together with Tables 1-3 allows the following conclusions to be drawn

(1) Average values of $\tilde{\gamma}_s$ and $\tilde{\phi}_s$ over the maximum slip depth of 5d may be used to construct the LFP concerning a deflection ~0.2d. The use of $\tilde{G}_s$ over a depth 14d is deemed appropriate.

(2) An average slope $\bar{\theta}_o$ was noted as 2.2% at y_o = 0.1d and 4% at y_o = 0.2d.

(3) Values of $P_t/\gamma_s d^3$ at y_o = 0.2d decrease linearly from 1,500 to 50, as the diameter d increases logarithmically from 10 to 1,000 mm (see Figure 17). Their values at y_o = 0.1d are constantly 30% low. Meanwhile, values of $M_{max}/\gamma_s d^4$ at y_o = 0.2d decrease linearly from 1,200 to 50 (see Figure 18), and reduced by 50% at y_o = 0.1d.

(4) Net resistance mobilized along 3 piles matches well with the Reese LFP (Reese et al. 1974), which are open ended pile PS1 (k_p = 6.5), reinforced H pile PS9 (k_p = 7), and bored aluminum (model) pipe pile PS14 (k_p = 3.5).

(5) Net resistance per unit length mobilized along 17 piles labeled as PSs2~8, 9~13, and 15~20 exceeds that obtained using Reese LFP. This is seen in the increase in N_g by:

- 400%, as noted for 5 piles of the reinforced pipe pile PSs8, 10, and H pile PS11 (k_p = 18~20) in Figure 12; the driven pile PS12 (k_p = 16) in Figure 13; and the open ended pipe pile PS15 (k_p = 26) in Figure 14. The limiting force along pile PSs8, 10 and 11 was mobilized to a depth of 1.5 ~2d; while along PSs 12 and 15, it was mobilized to a depth of 5.7d and 4.3d, respectively.
- 150~350%, as observed for 10 piles (see Table 2), including pile PSs3 (k_p = 27), 6 (11), PSs16 and 18 (k_p = 18~20). The corresponding slip depths are 1.7d, 3.6d, 4.3d, and 2d, respectively. The LFPs along the pile PSs16 and 18 may alter slightly, if bending moment is provided.

In addition, the gradient of the resistance, N_g mobilized along the reinforced pipe pile PSs8, 10, and the large cross-sectional area (of 21154.8 mm^2) H pile PS11 was 200~230% (or 200~220% in k_p) that along the pipe pile PS7. The N_g is 330~370% (or 285~314% in k_p) that along the low cross-sectional area (of 16580.6 mm^2), reinforced H pile PS9 (see Figures 8-12).

The back-estimation was generally based on an excellent match with measured data of one curve (for 8 piles of PS9, 14~20) or three curves (all other piles). The deduced magnitudes are similar to those obtained for free-head piles in calcareous sand (Guo and Zhu 2005).

5.2 Comments

The back estimation allows the following comments to be made:

- The average $\overline{N}_g$ for all piles investigated is $1.29K_p^2$, which is 29% higher than that suggested previously (Barton 1982), (Zhang et al. 2002).
- The power of n = 1.7 deduced from COM624P (FHWA 1993) exceeds n = 1 suggested for rigid piles, reflecting the influence of the pile flexibility.
- A ~400% higher limiting force was noted for 17 out of 20 piles. It was mobilised to a shallower depth than that obtained using the conventional suggestions. The later suggestions may render pile displacement to be overestimated, and maximum bending moment to be underestimated. Nevertheless, the conventional suggestions may still be appropriate for piles in groups, as the gradient of a LFP along a fixed-head pile is as low as 25 % that for a free-head pile addressed herein(Guo 2005; Guo 2009). This outcome is in a sharp contrast with the likely over-design for free-head piles in clay using the existing (other than Hansen's) methods.
- The alterative Equation (6) may be used for constructing the LFP, where apparent cohesion does not exist. Reese's LFP may be obtained using k_p = 6.5~7.5, and it is suitable for loose, and/or submerged sand. The k_p increases to 16~27 for reinforced pipe piles in medium ~ dense sand.
- The apparent cohesion ($\alpha_o \neq 0$) observed around the wet driven pile PS3 may be incorporated (Guo 2005) to improve the accuracy of back-estimation, as is the case for PS4.

- Equation (6) capture the main impact of pile-soil relative stiffness via increase n from 1.0 to 1.35; of dilatancy via increase n from 1.35 to 1.52; of non-homogeneous layer via employing n > 1.7; of 'free water' via the ratio γ/γ_s; of depth via the ratio x/d; of pile diameter via d^{n_p}; and of types of piles and installation procedure via the value k_p.

Guo (2005b, 2006) (Guo 2005; Guo 2006) validates the current back-estimation procedure, and concludes that: Input parameters are uniquely deduced, should identical parameters such as γ_s, ϕ_s and n be adopted, which warrant an optimised match between the measured and predicted (three) response of piles. This is, however, difficult to achieve in practice, especially with less than 3 measured curves available. Nevertheless, a similar total resistance is observed over the respective slip depth, regardless of the 'significant' difference in values of input parameters. The conclusion (Guo 2006) is seen in Case III. Given the complexity for each case, the current study is deemed sufficiently accurate. Use of the LFP to estimate response of a free head pile is exemplified previously (Guo 2006).

6 CONCLUSIONS

Input parameters for laterally loaded piles were deduced against 20 tested piles, which shows that:

(1) $G_s = (0.25 \sim 0.62)N$ (MPa) with $\overline{G}_s = 0.5N$ (MPa); $k = (2.4\sim3.7)G_s$ with $\bar{k} = 3.2G_s$.

(2) Using Equation (3) to construct LFP may generally be based on n = 1.7, $\alpha_o = 0$, and $N_g = (0.4\sim2.8)K_p^2$ but a high n is anticipated for a shape strength increase profile (PS3). In contrast, using Equation (6) may be based on n = 1.52 and k_p = 6.5~15. High k_p (> 15) should only be used with caution and for high displacement pipe-piles in medium and dense sand, and,

(3) Equation (3) is intended for any subsoils, whereas Equation (6) is suitable for piles in sand only and linked to pipelines.

The deduced LFP generally has a higher gradient than that obtained using existing methods. It is legitimate for free-head piles compared to pipelines. The gradient should be reduced for capped piles. Not all cases investigated herein are typical, but the results are quite consistent.

REFERENCES

Alizadeh, M. and Davisson, M. T. (1970). Lateral load test piles, Arkansas river project. Journal of Soil Mechanics and Foundation Engineering Division, American Society of Civil Engineers **96**(5): 1583-1604.

Barton, Y. O. (1982). Laterally loaded model piles in sand: Centrifuge tests and finite element analysis, University of Cambridge. Ph. D Thesis.

Broms, B. (1964). Lateral resistance of piles in cohesionless soils. Journal of Soil Mechanics and Foundation Engineering Division, American Society of Civil Engineers **90**(3): 123-56.

Brown, D. A., Morrison, C. and Reese, L. C. (1988). Lateral load behaviour of pile group in sand. Journal of Geotechnical and Geoenvironmental Engineering, American Society of Civil Engineers **114**(11): 1261-1276.

Cox, W. R., Reese, L. C. and Grubbs, B. R. (1974). Field testing of laterally loaded piles in sand. *In* Proceedings 6th International Offshore Technology Conference Houston, Texas, paper number OTC 2079.

Fan, C.-C. and Long, J. H. (2005). Assessment of existing methods for predicting soil response of laterally loaded piles in sand. Computers and Geotechnics **32**(4): 274-289.

FHWA (1993). COM624P-laterally loaded pile analysis program for the microcomputer. Report No. FHWA-SA-91-048. Washington, D. C., USA.

Gandhi, S. R. and Selvam, S. (1997). Group effect on driven piles under lateral load. Journal of Geotechnical and Geoenvironmental Engineering, American Society of Civil Engineers **123**(8): 702-709.

Gill, H. L. (1969). Soil-pile interaction under lateral loading. Technical Report R-670. California, U. S. Naval Civil Engineering Laboratory. 2005.

Guo, P. J. and Stolle, D. F. E. (2005). Lateral pipe-soil interaction in sand with reference to scale effect. Journal of Geotechnical and Geoenvironmental Engineering, American Society of Civil Engineers **131**(3): 338-349.

Guo, W. D. (2001). Lateral pile response due to interface yielding. *In* Proceedings 8th International Conference Civil and Structural Engineering Computing, Eisenstadt, nr Vienna, Austria, Civil-Comp press, Stirling, United Kingdom.

Guo, W. D. (2001). Subgrade modulus for laterally loaded piles. *In* Proceedings 8th International Conference Civil and Structural Engineering Computing, Eisenstadt, nr Vienna, Austria, Civil-Comp press, Stirling, United Kingdom.

Guo, W. D. (2003). Response of laterally loaded rigid piles. *In* Proceedings of 12th Pan-American conference on soil mechanics and Geotechnical engineering, Cambridge, Massachusettes, USA, Verlag Gluckauf GmbH

Guo, W. D. (2004). Laterally loaded rigid piles in Gibson soil. *In* Proceedings 2rd International Conference on Structural Engineering Mechanics and Computation, Cape Town, South Africa.

Guo, W. D. (2005). Limiting force profile and laterally loaded pile groups. *In* Proceedings 6th International conference on Tall Buildings, Hong Kong, China, World Scientific.

Guo, W. D. (2006). On limiting force profile, slip depth and lateral pile response. Computers and Geotechnics **33**(1): 47-67.

Guo, W. D. (2008). Laterally loaded rigid piles in cohesionless soil. Canadian Geotechnical Journal **45**(5): 676-697.

Guo, W. D. (2009). Non-linear response of laterally loaded piles and pile groups. International Journal for Numerical and Analytical Methods in Geomechanics(in press): DOI:10.1002/nag.746.

Guo, W. D. and Lee, F. H. (2001). Load transfer approach for laterally loaded piles. International Journal for Numerical and Analytical Methods in Geomechanics **25**(11): 1101-1129.

Guo, W. D. and Zhu, B. T. (2005). Limiting force profile for laterally loaded piles in clay. Australian Geomechanics **40**(3): 67-80.

Guo, W. D. and Zhu, B. T. (2005). Static and cyclic behaviour of laterally loaded piles in calcareous sand. *In* International Symposium on Frontiers in Offshore Geotechnics, Perth, Australia, Taylor & Francis/Balkema.

Hansen, B. J. (1961). The ultimate resistance of rigid piles against transversal forces. Copenhagen, Denmark, The Danish Geotechnical Institute Bulletin No. 12: 5-9.

Kishida, H. and Nakai, S. (1977). Large deflection of a single pile under horizontal load. *In* Proceedings 9th International Conference on Soil Mechanics and Foundation Engineering, Speciality session 10, Tokyo.

Kulhawy, F. H. and Mayne, P. W. (1990). Manual on estimating soil properties for foundation design. Report No. EL-680. Ithaca, N. Y., Electric Power Research Institute. 2005.

Matlock, H. (1970). Correlations for design of laterally loaded piles in soft clay. *In* Proceedings 2nd Annunal Offshore Technology Conference, OTC1204, Dallas, Texas.

McVay, M., Casper, R. and Shang, T. L. (1995). Lateral response of three-row groups in loose to dense sands at 3D and 5D pile spacing. Journal of Geotechnical Engineering, American Society of Civil Engineers **121**(5): 436-441.

Murff, J. D., Wagner, D. A. and Randolph, M. F. (1989). Pipe penetration in cohesive soil. Geotechnique **39**(2): 213-229.

Nakai, S. and Kishida, H. (1982). Nonlinear analysis of a laterally loaded pile. *In* Proceedings 4th International Conference on Numerical Methods in Geomechanics, Edmonton.

Rajani, B. B. and Morgenstern, N. R. (1993). Pipelines and laterally loaded piles in elastoplastic medium. Journal of Geotechnical Engineering, American Society of Civil Engineers **119**(9): 1431-1447.

Randolph, M. F. and Houlsby, G. T. (1984). The limiting pressure on a circular pile loaded laterally in cohesive soil. Geotechnique **34**(4): 613-623.

Randolph, M. F., Jewell, R. J. and Poulos, H. G. (1988). Evaluation of pile lateral load performance. *In* Proceedings of Engineering for Calcareous Sediments, Perth, Australia, Balkema, Rotterdam.

Reese, L. C., Cox, W. R. and Koop, F. D. (1974). Analysis of laterally loaded piles in sand. *In* Proceedings 6th Annunal Offshore Technology Conference, OTC. 2080, Dallas, Texas.

Reese, L. C. and Van Impe, W. F. (2001). Single piles and pile groups under lateral loading. Rotterdam, A. A. Balkema.

Rollins, K. M., Lane, J. D. and Gerber, T. M. (2005). Measured and computed lateral resistance of a pile group in sand. Journal of Geotechnical and Geoenvironmental Engineering, American Society of Civil Engineers **131**(1): 103-114.

Zhang, L., Silva-Tulla, F. and Grismala, R. (2002). Ultimate resistance of laterally loaded piles in cohesionless soils. *In* Proceedings International Deep Foundations Congress, 2002; An international perspective on theory, design, construction, and performance., Orlando, Florida, American Society of Civil Engineers.

Table 1 Summary of properties of piles and sands

Pile	Reference		Pile type	L (m)	d/t (mm)	E_p(GPa)	E_pI_p (MNm^2)	e (m)[a]	γ_s (kN/m^3)[f]	SPT N	G_s (MPa)
PS1	Cox, et al (1974)	Mustang	Open ended pipe pile	21.05	610/9.53	24.0	163	0.305	10.4	18	10.5
PS2	Brown, et al. (1988)	Single pile	Open ended pipe pile	13.12	273/9.27	50.3	13.708	0.305	15.4	35	16.5
PS3	Kishida & Nakai (1977)	Pile C	Driven pipe pile	23.5	609.6	24.5	166.04	0.2	16.5	12	3.23
PS4		Pile D		44.0	812.8	24.6	527.4	0.6	17.0[c]	9	4.15
PS5	Nakai & Kishida (1982)	Pile A	Pipe pile	1.8	60.5/2.3	55.1	3.626×10^{-2}	0.12	18.0[c]	27	5.0
PS6	Rollins et al. (2005)	Single pile	Driven open-ended pipe pile	11.5	324/9.5	52.9	28.6	0.69	10.3	10	6.15
PS7	Alizadeh & Davisson (1970)	Pile 16	Open ended pipe pile	16.07	406.4/7.9	51.5	69.016	0.0	9.87	12	9.54
PS8[b]		Pile 2	Reinforced pipe pile	16.10	480.3/7.9	26.7	69.877	0.031	10.9	12	11.8
PS9[b]		Pile 6	Reinforced H pile (14BP73)	12.2	444.8[e]	32.1	61.698	0.031	9.87	12	16.6
PS10[b]		Pile 10	Reinforced pipe pile	16.20	480.3/7.9	26.7	69.877	0.107	9.87	12	16.6
PS11[b]		Pile 13A	Reinforced H pile	12.96	434.5[e]	40.7	71.225	0.153	9.87		6.65
PS12	Gandhi & Selvam (1997)	Model tests	Driven aluminum pipe pile	0.5	18.2/0.75	16.0	8.6×10^{-5}	0.01	16.22		0.45
PS13[c]								0.01			0.45
PS14[c]			Bored pipe pile					0.047[d]			0.3
PS15	Gill (1969)	Pile 9	Open ended pipe pile	5.537	120.6	59.9	0.623	0.813	19.63	29.2	18.0
PS16		Pile 10		7.315	218.9	55.2	6.227	0.813	19.63	26.9	16.6
PS17		Pile 11		9.296	323.9	39.6	21.408	0.813	19.63	24.9	11.5
PS18		Pile 12		9.296	406.4	36.2	48.497	0.813	19.63	24.9	11.5
PS19	McVay et al. (1995)	Centrifuge tests	Open ended pipe pile	11.1	430	43.0	72.1	2.2	15.18		6.0
PS20									14.51		3.2

[a] Free length e was taken as the height of the top of the pile cap

[b] Using $\phi_s = 43^o$ (Reese and Van Impe 2001) rather than $\phi_s = 35^o$ (Alizadeh and Davisson 1970). An enlarged diameter 480.3 mm for PS8 was used instead of the OD of inner pipe pile. Using $\phi_s = 35^o$, the obtained s_g will be doubled.

[c] Assumed ones; [d]: PSs 13 and 14 are fixed-head, while all other pile are free-head. The response of the latter was checked using a finite difference program. [e] Equivalent diameter; [f] Effective unit weight (see Equations (3) and (5)).

Note: 1. Water tables were at or above the groundline for PS1~2 and PS6~11, at 1.4 m below the groundline for PS15~18, below the pile bases (dry sand) for PS12~14, PS19 and 20; and unknown for PS3~5. 2. The friction angle for PS1 exceeds that of PS2, due to the driving action, whereas sand was placed and compacted around PS2. And 3. Behaviour of lateral piles is controlled by top soil (up to 10d), stiff clay over some of the pile length and layered soils were not discussed.

Table 2 Input parameters for the investigated piles

Case	Soil type	N_g/K_p^2	G_s/N (MPa)	k/G_s [a]	Times [b]	k_p [c]	γ/γ_s	s_g [c]
PS1	Submerged dense sand	0.93	0.58	3.55	1.0	6.5	1.94	0.740
PS2	Submerged firm to dense sand	0.66	0.47	2.98	1.8	13	1	0.973
PS3	Medium dense sand	2.5	0.27	3.22	3.0	27	1	2.98
PS4	Loose sand	1.1	0.46	3.28	1.7	11	1	1.329
PS5	Medium dense sand	*0.85*		3.12	2.0	11	1	1.255
PS6	Submerged medium dense sand	1.5	0.62	3.18	3.5	11	1.95	2.036
PS7	Submerged medium dense sand	0.78	0.35	3.30	1.6	10	1.993	0.892
PS8	Submerged medium dense sand	1.6	0.58	3.56	4.0	18	1.899	1.631
PS9	Submerged medium dense sand	0.49	0.62	3.61	1.0	7	1.993	0.611
PS10	Submerged medium dense sand	1.6	0.62	3.73	4.0	19	1.993	1.711
PS11	Submerged medium dense sand	1.8	0.25	3.27	4.0	20	1.993	1.93
PS12	Medium dense sand	2.0		2.86	4.0	16	1	2.861
PS13		*1.0*		2.44	2.1	8.0	1	1.430
PS14		0.4		2.38	1	3.5	1	0.625
PS15	Compacted granular soil	2.8	0.62	3.44	4.0	26	1	3.52
PS16	Compacted granular soil	1.8	0.62	3.44	2.5	20	1	2.43
PS17	Compacted granular soil	1.1	0.46	3.43	2.0	13	1	1.51
PS18	Compacted granular soil	1.5	0.46	3.46	3.0	18	1	1.97
PS19	Medium dense sand	0.65		3.23	2.0	14	1	0.895
PS20	Loose sand	0.8		3.07	1.5	10	1	0.987
Average value		1.29	0.5	3.23				1.594

$n = 1.7$, $\alpha_0 = 0$, and $n_p = 0.25$ for all cases. [a]: (Guo and Lee 2001); [b]: A_L for Guo's LFP/A_L for Reese's LFP; [c]: $s_g = (\gamma/\gamma_s)k_p/(d^{n_p}K_p^2)$. The deduced s_g herein is different from the s_g of N_g/K_p^2 for n = 1.7, shown in figures.

Table 3 Derived response of pile in sand

Case	L_c/d	y_o/d =10%					y_o/d =20%				
		$P_t/\gamma_s d^3$	x_p/d	θ_o (%)	$M_{max}/\gamma_s d^4$	x_{max}/d	$P_t/\gamma_s d^3$	x_p/d	θ_o (%)	$M_{max}/\gamma_s d^4$	x_{max}/d
PS1	7.3	180.06	4.07	2.46	631.52	4.12	270.20	5.03	4.49	1079.44	4.79
PS2	7.8	327.76	5.18	2.06	1535.44	4.89	488.93	6.33	3.71	2568.93	5.67
PS3	9.8	119.05	1.63	2.21	290.41	3.63	202.65	2.22	4.37	555.53	3.85
PS4	9.2	80.63	2.46	2.30	252.14	3.60	130.69	3.23	4.39	462.27	4.01
PS5	8.6	677.34	6.16	1.74	4099.37	5.58	1011.79	7.50	3.13	6782.80	6.47
PS6	10.1	345.68	3.66	1.93	1767.93	4.17	548.92	5.86	3.58	3108.65	4.85
PS7	9.0	464.60	3.99	2.19	1525.90	4.62	707.27	5.02	4.09	2704.70	5.26
PS8	7.2	407.05	2.82	2.82	1008.01	3.44	629.05	3.58	5.31	1806.40	3.89
PS9	7.0	325.56	4.81	2.43	1128.69	4.66	477.16	5.85	4.38	1900.67	5.37
PS10	6.7	468.82	3.31	2.95	1284.06	3.46	704.99	4.10	5.41	2219.89	4.01
PS11	9.3	454.04	2.48	2.28	1280.77	3.79	733.51	3.25	4.40	2363.43	4.17
PS12	14.0	772.63	3.35	1.45	2901.14	6.10	1266.58	4.46	2.85	5474.73	6.55
PS13	14.4	1142.86	4.78	0.57	-7686.03 (2112.75)	0 (9.89)	1881.96	6.43	1.03	-13143.92 (4045.13)	0 (10.34)
PS14	15.9	771.8	5.98	0.45	-5649.92 (1584.96)	0 (11.24)	1245.12	8.09	0.80	-9920.68 (2977.56)	0 (11.99)
PS15	8.0	421.36	4.32	1.90	3957.64	3.64	663.21	5.35	3.38	6551.48	4.31
PS16	8.0	300.94	4.21	2.03	1969.66	3.88	467.81	5.24	3.66	3297.04	4.57
PS17	8.0	181.47	3.94	2.15	966.95	3.86	281.48	4.93	3.90	1639.97	4.54
PS18	7.9	178.56	3.28	2.37	803.31	3.43	280.17	4.15	4.34	1387.36	4.04
PS19	9.7	121.30	3.24	2.00	916.83	3.35	197.45	4.16	3.64	1587.65	4.01
PS20	11.3	99.86	2.96	1.85	758.73	3.49	166.17	3.88	3.41	1346.20	4.11

Figure Captions

Figure 1 Schematic coupled load transfer analysis for a free-head pile (Guo 2001; Guo 2006): (a) The problem addressed ($L > L_c$+ 8~20d); (b) Coupled load transfer model, and (c) Load transfer (p-y) curve

Figure 2 Predicted vs measured (Reese et al. 1974) response of pile PS1, in Mustang: (a) p_u profiles, (b) P_t-y_t and P_t-M_{max} curves, (c) P_t-θ_o curves, and (d) M profiles under P_t = 210 kN

Figure 3 Predicted vs measured (Brown et al. 1988) responses of pile PS2: (a) p_u profiles, (b) P_t-y_t curves , and (c) M profiles

Figure 4 Predicted vs measured (Kishida and Nakai 1977) (Pile C) responses of pile PS3: (a) p_u profiles, (b) P_t-y_o and P_t-M_{max} curves, and (c) P_t-x_{max}

Figure 5 Predicted vs measured (Kishida and Nakai 1977) (Pile D) responses of pile PS4: (a) p_u profiles, (b) P_t-y_o and P_t-M_{max} curves, and (c) M_{max}-x_{max}

Figure 6 Predicted vs measured (Nakai and Kishida 1982) (Pile A) responses of pile PS5: (a) p_u profiles, (b) P_t-y_t curves , and (c) M profiles

Figure 7 Predicted vs measured (Rollins et al. 2005) responses of pile PS6: (a) p_u profiles, and (b) P_t-y_t and P_t-M_{max} curves

Figure 8 Predicted vs measured (Alizadeh and Davisson 1970) responses of pile PS7: (a) P_t-y_o and P_t-M_{max} curves, and (b) M profiles

Figure 9 Predicted vs measured (Alizadeh and Davisson 1970) responses of pile PS8(a) P_t-y_o and P_t-M_{max} curves, and (b) M profiles

Figure 10 Predicted vs measured (Alizadeh and Davisson 1970) responses of pile PS10: (a) P_t-y_o and P_t-M_{max} curves, and (b) M profiles

Figure 11 Predicted vs measured (Alizadeh and Davisson 1970) responses of pile PS11: (a) P_t-y_o and P_t-M_{max} curves, and (b) M profiles

Figure 12 Predicted vs measured (Alizadeh and Davisson 1970) responses of pile PS9 and LFPs for PSs7-8, and 10-11: (a) p_u profiles, and (b) P_t-y_o curves

Figure 13 Predicted vs measured (Gandhi and Selvam 1997) responses of pile PSs12-14: (a) p_u profiles, (b) P_t-y_t curves, and (c) M profile

Figure 14 Predicted vs measured (Gill 1969) responses of pile PSs15-18 in San Francisco: (a) p_u profiles, and (b) P_t-y_o curves

Figure 15 Predicted vs measured (McVay et al. 1995) responses of pile PS19: (a) p_u profiles, and (b) P_t-y_t curves

Figure 16 Predicted vs measured (McVay et al. 1995) responses of pile PS20: (a) p_u profiles, and (b) P_t-y_t curves

Figure 17 $P_t/\gamma_s d^3 \sim d$ relationship (20 piles)

Figure 18 $M_{max}/\gamma_s d^4 \sim d$ relationship (20 piles)

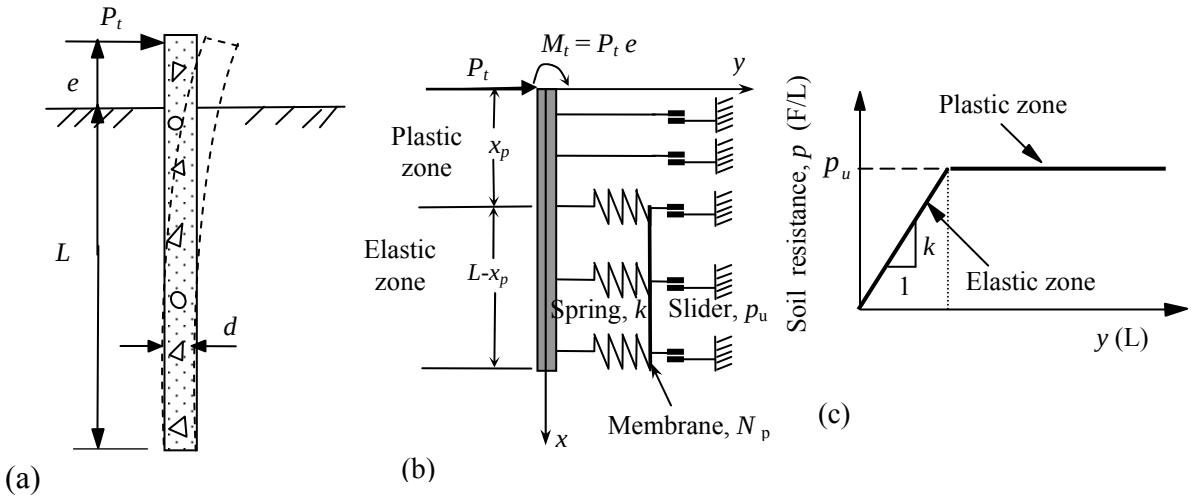

Figure 1: Schematic coupled load transfer analysis for a free-head pile (Guo 2001; Guo 2006): (a) The problem addressed ($L > L_c + 8\sim20d$); (b) Coupled load transfer model, and (c) Load transfer (p-y) curve

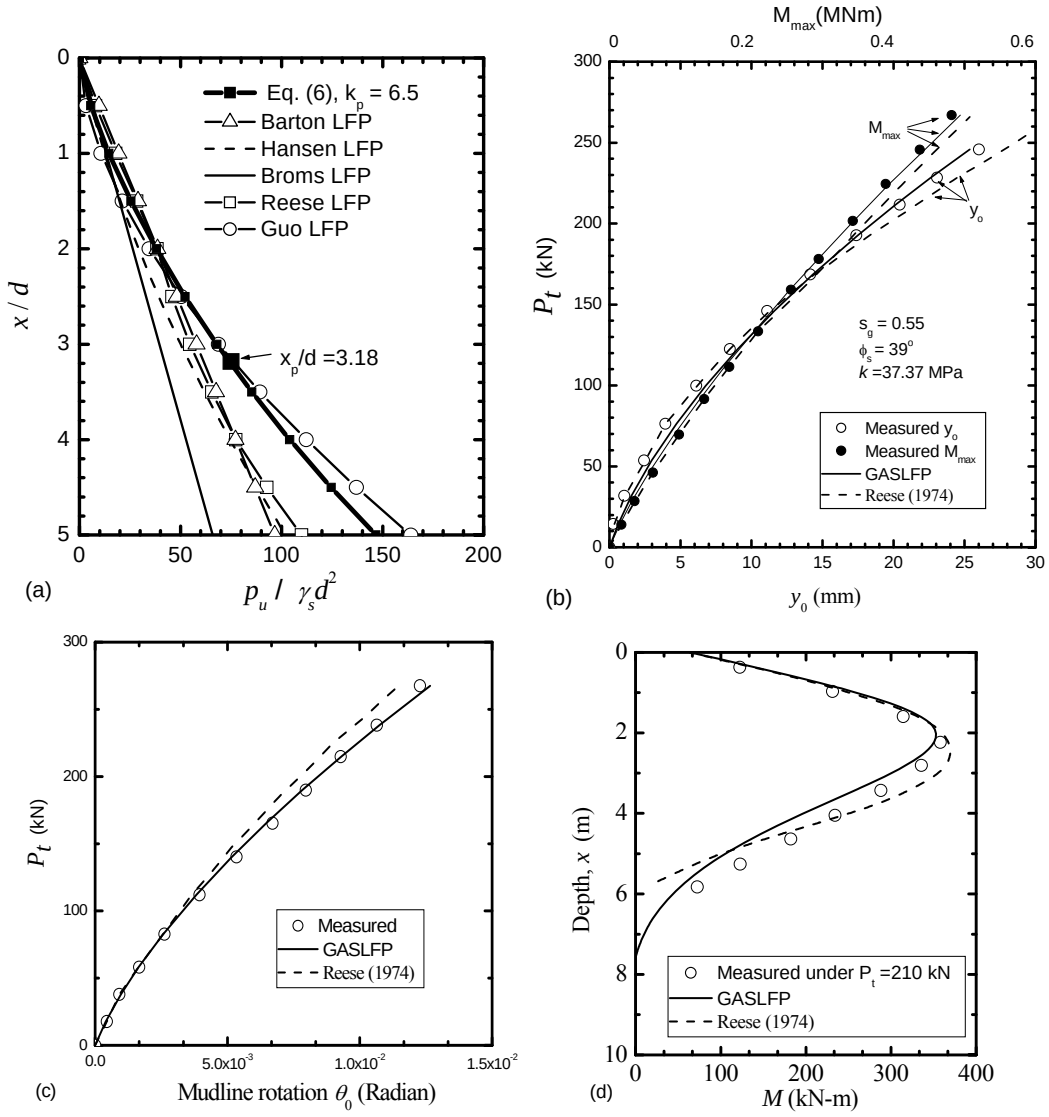

Figure 2: Predicted vs measured (Reese et al. 1974) response of pile PS1, in Mustang: (a) p_u profiles, (b) P_t-y_t and P_t-M_{max} curves, (c) P_t-θ_o curves, and (d) M profiles under P_t = 210 kN

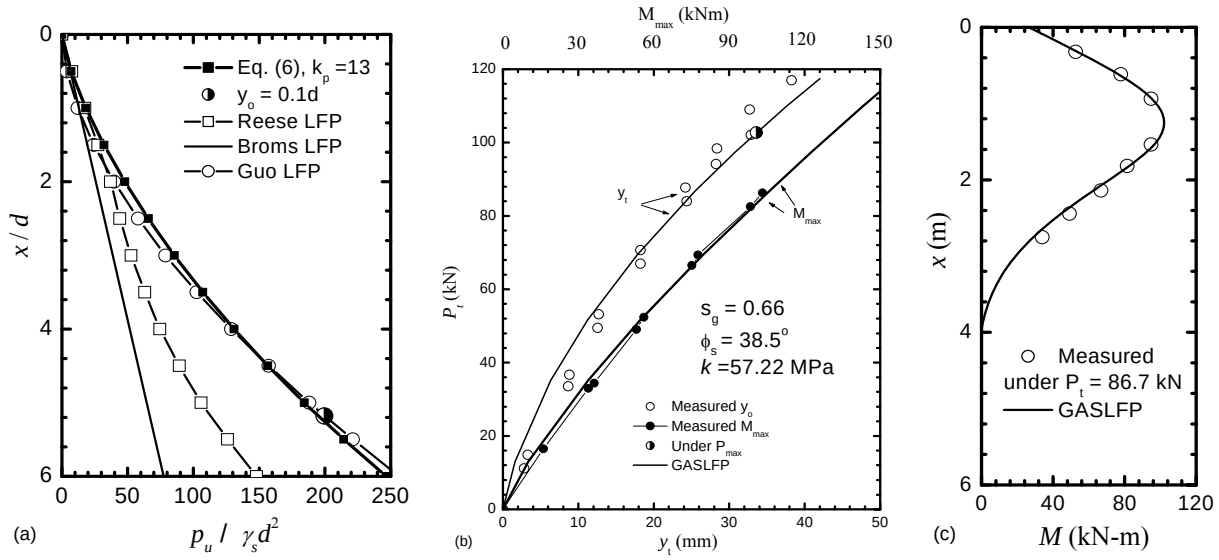

Figure 3: Predicted vs measured (Brown et al. 1988) responses of pile PS2: (a) p_u profiles, (b) P_t-y_t curves , and (c) M profiles

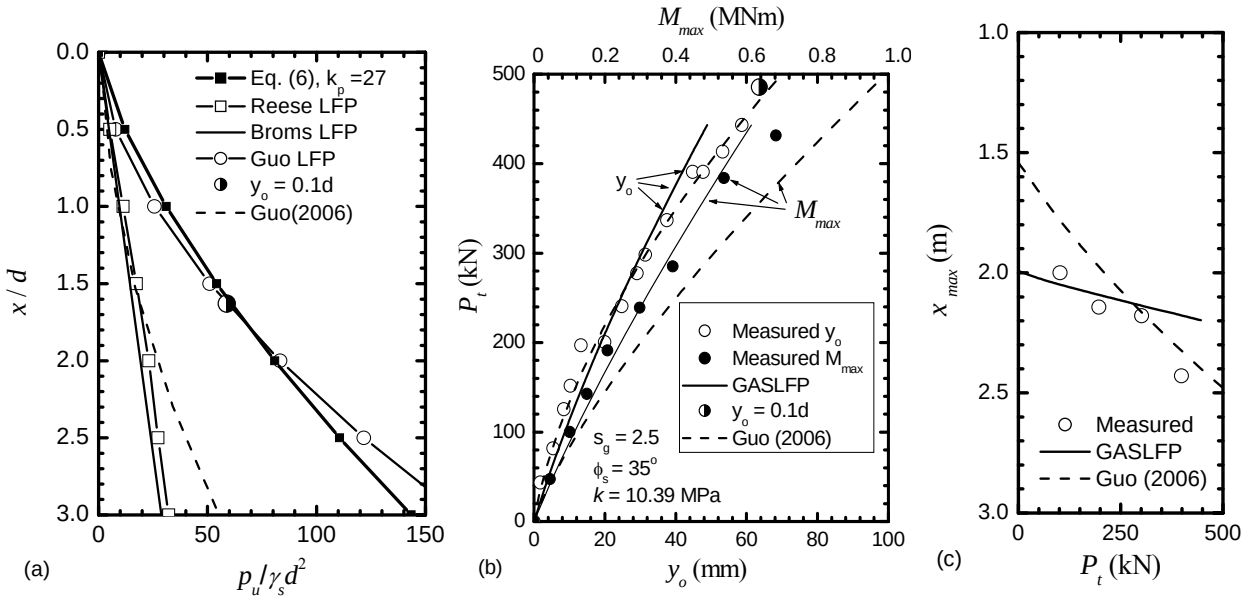

Figure 4: Predicted vs measured (Kishida and Nakai 1977) (Pile C) responses of pile PS3: (a) p_u profiles, (b) P_t-y_o and P_t-M_{max} curves, and (c) P_t-x_{max}

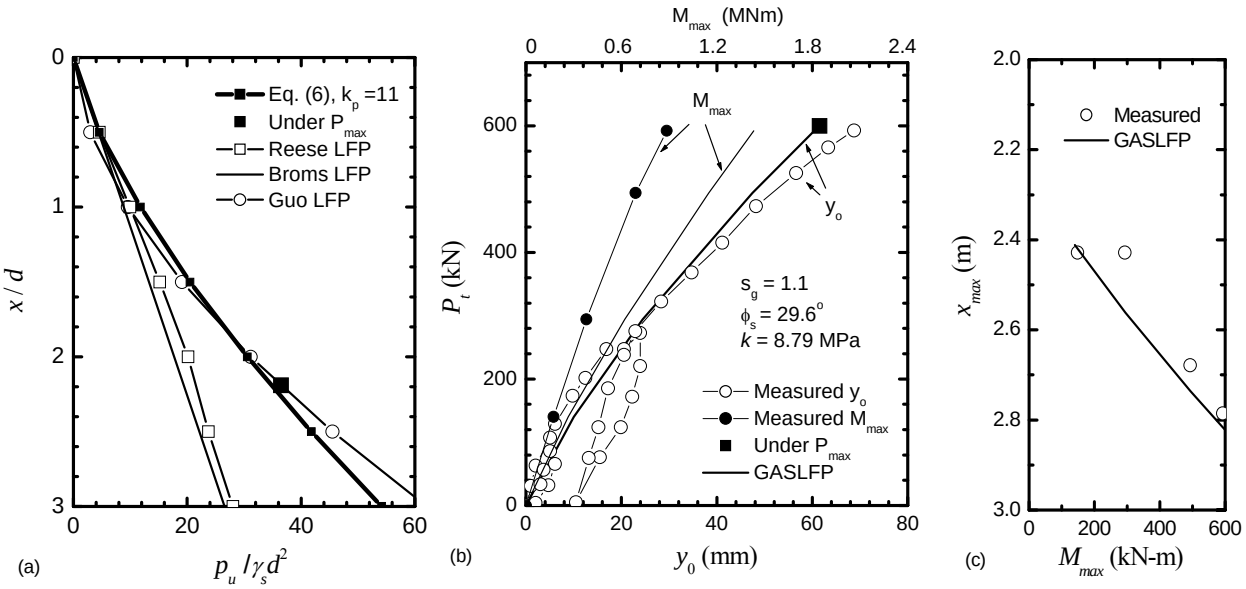

Figure 5: Predicted vs measured (Kishida and Nakai 1977) (Pile D) responses of pile PS4: (a) p_u profiles, (b) P_t-y_o and P_t-M_{max} curves, and (c) M_{max}-x_{max}

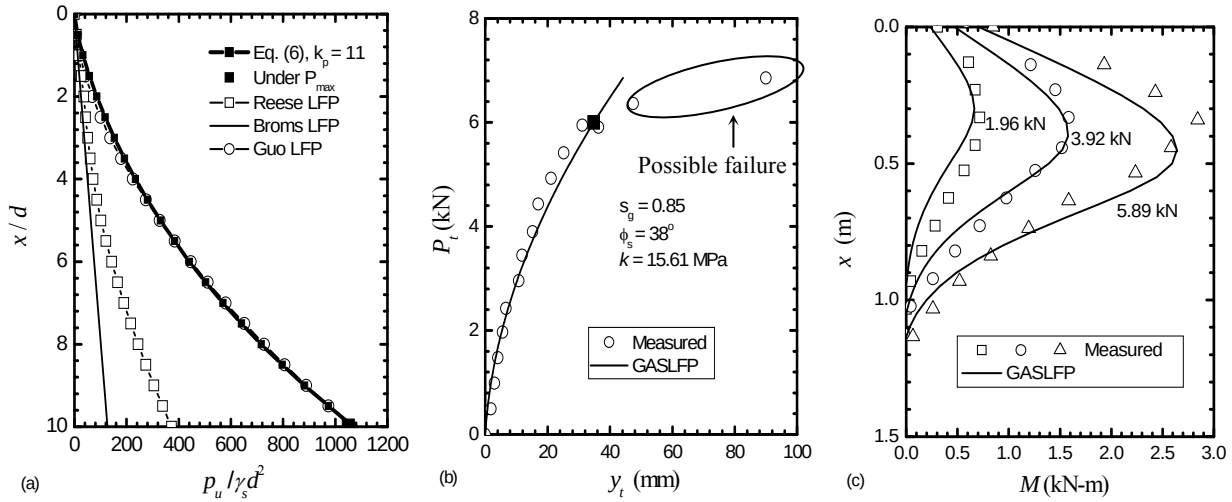

Figure 6: Predicted vs measured (Nakai and Kishida 1982) (Pile A) responses of pile PS5: (a) p_u profiles, (b) P_t-y_t curves , and (c) M profiles

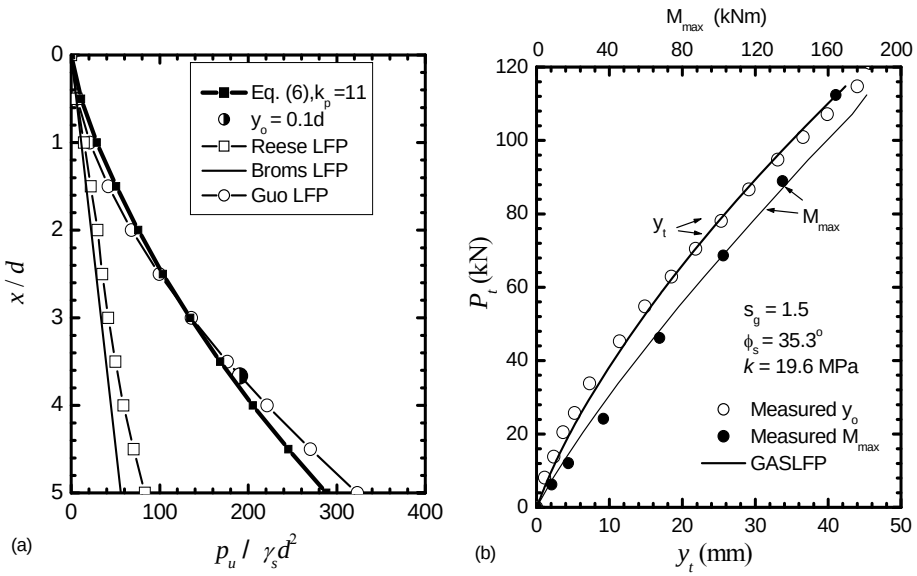

Figure 7: Predicted vs measured (Rollins et al. 2005) responses of pile PS6: (a) p_u profiles, and (b) P_t-y_t and P_t-M_{max} curves

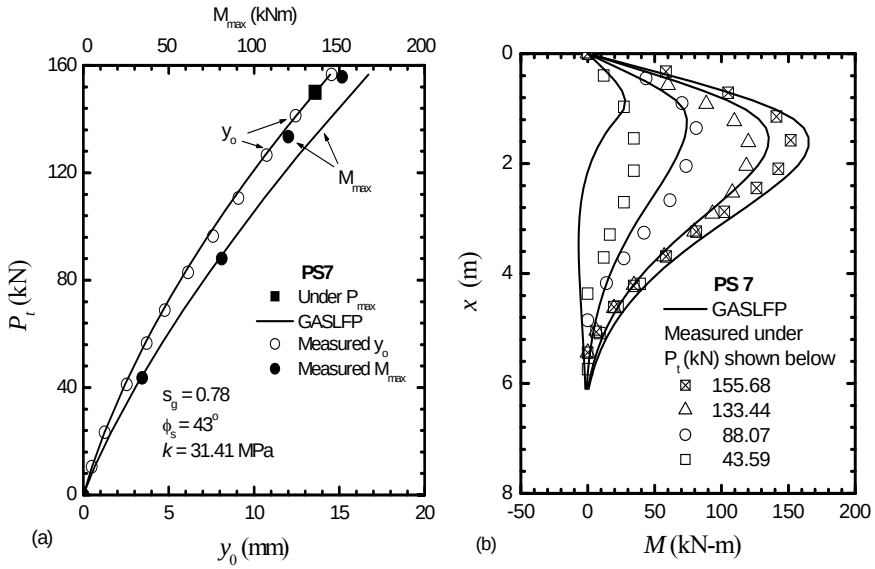

Figure 8: Predicted vs measured (Alizadeh and Davisson 1970) responses of pile PS7: (a) P_t-y_o and P_t-M_{max} curves, and (b) M profiles

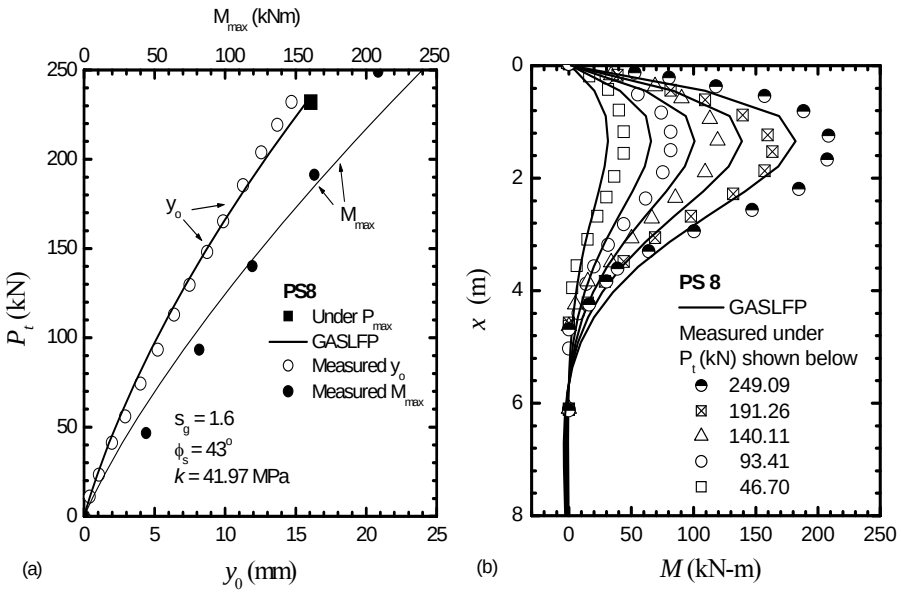

Figure 9: Predicted vs measured (Alizadeh and Davisson 1970) responses of pile PS8: (a) P_t-y_o and P_t-M_{max} curves, and (b) M profiles

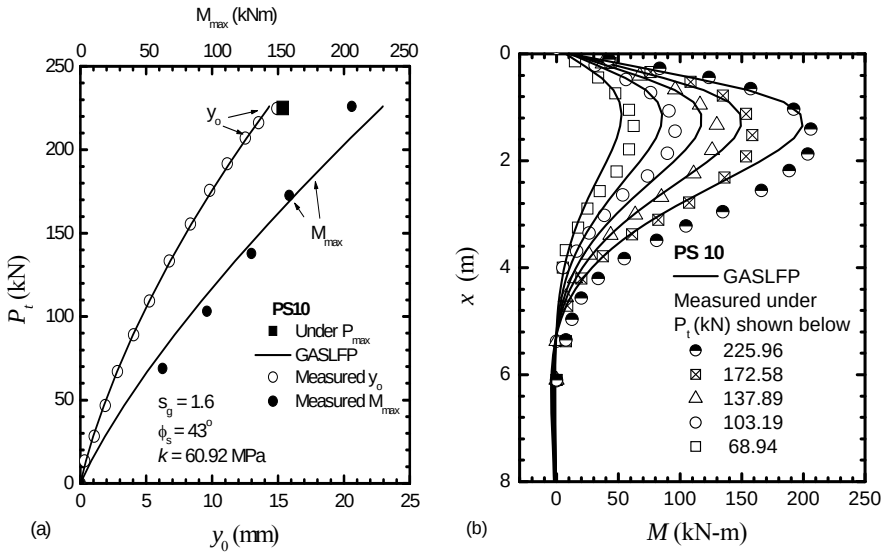

Figure 10: Predicted vs measured (Alizadeh and Davisson 1970) responses of pile PS10: (a) P_t-y_o and P_t-M_{max} curves, and (b) M profiles

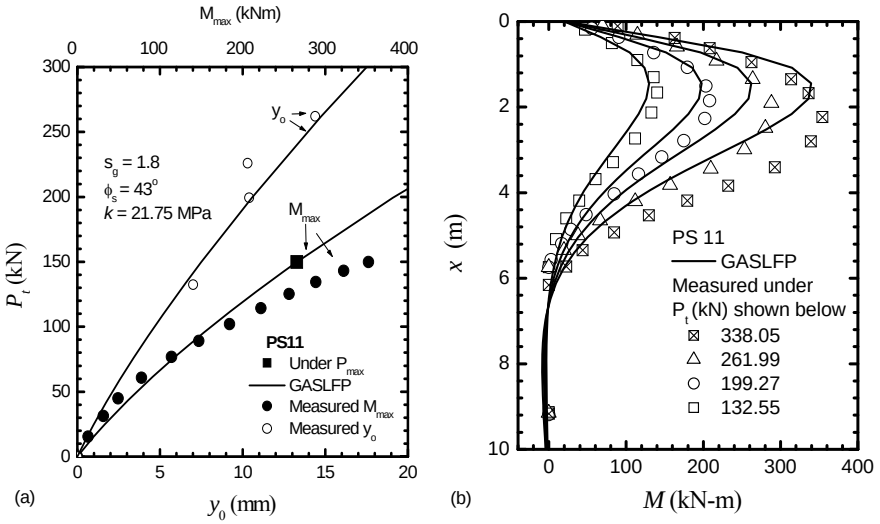

Figure 11: Predicted vs measured (Alizadeh and Davisson 1970) responses of pile PS11: (a) P_t-y_o and P_t-M_{max} curves, and (b) M profiles

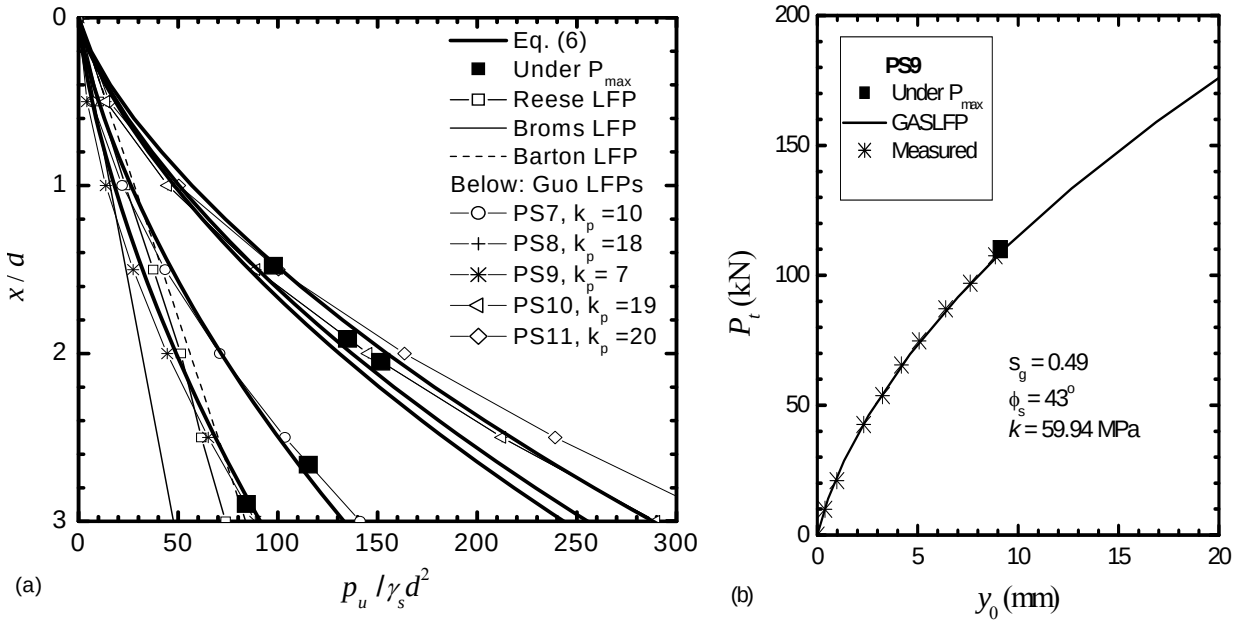

Figure 12: Predicted vs measured (Alizadeh and Davisson 1970) responses of pile PS9 and LFPs for PSs7-8, and 10-11: (a) p_u profiles, and (b) P_t-y_o curves

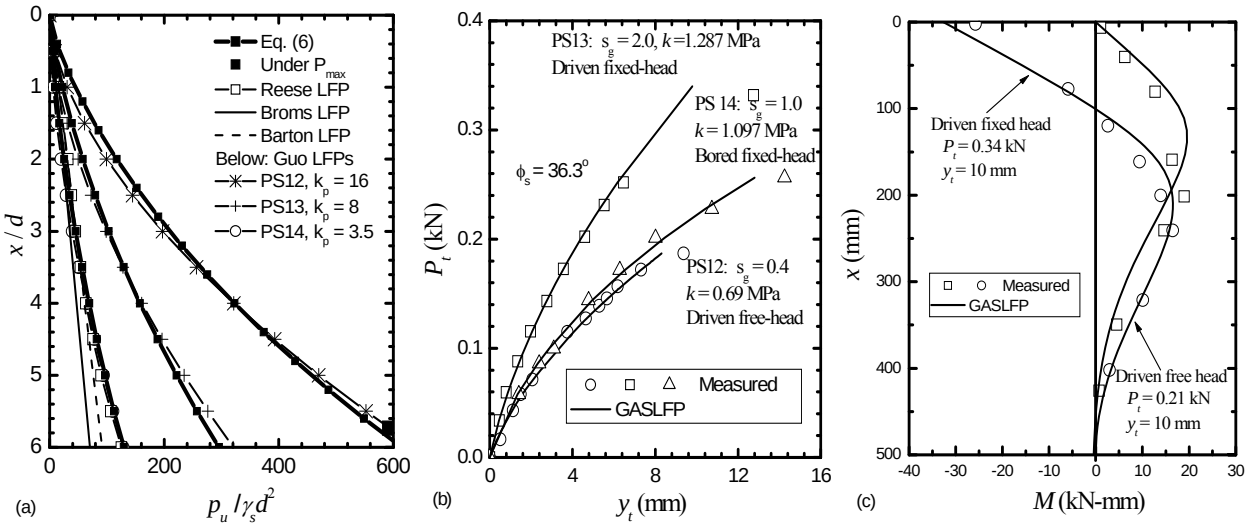

Figure 13: Predicted vs measured (Gandhi and Selvam 1997) responses of pile PSs12-14: (a) p_u profiles, (b) P_t-y_t curves, and (c) M profile

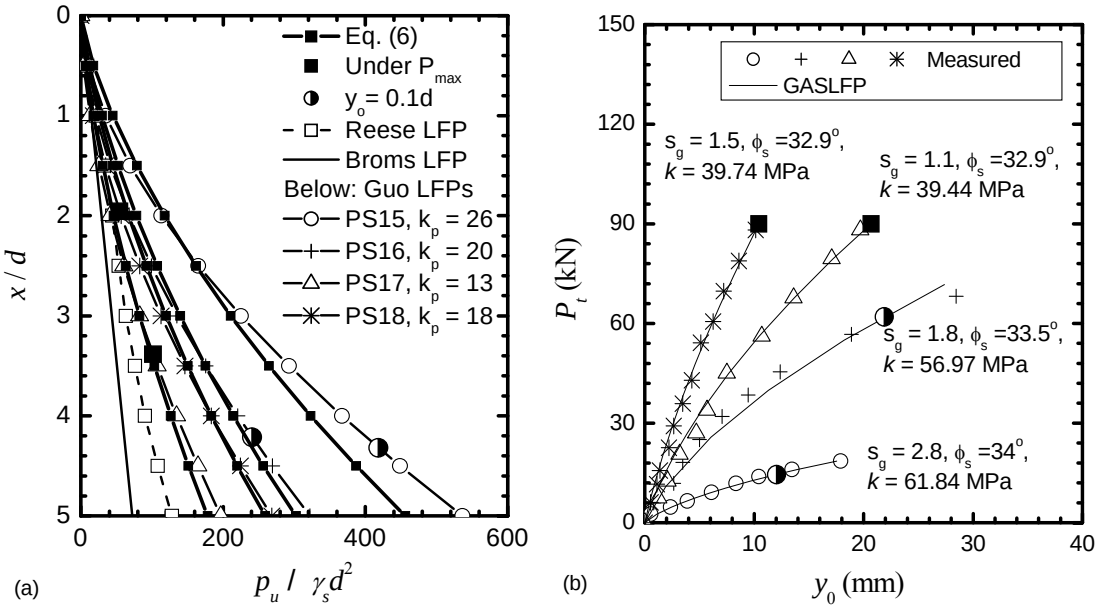

Figure 14: Predicted vs measured (Gill 1969) responses of pile PSs15-18 in San Francisco: (a) p_u profiles, and (b) P_t-y_o curves

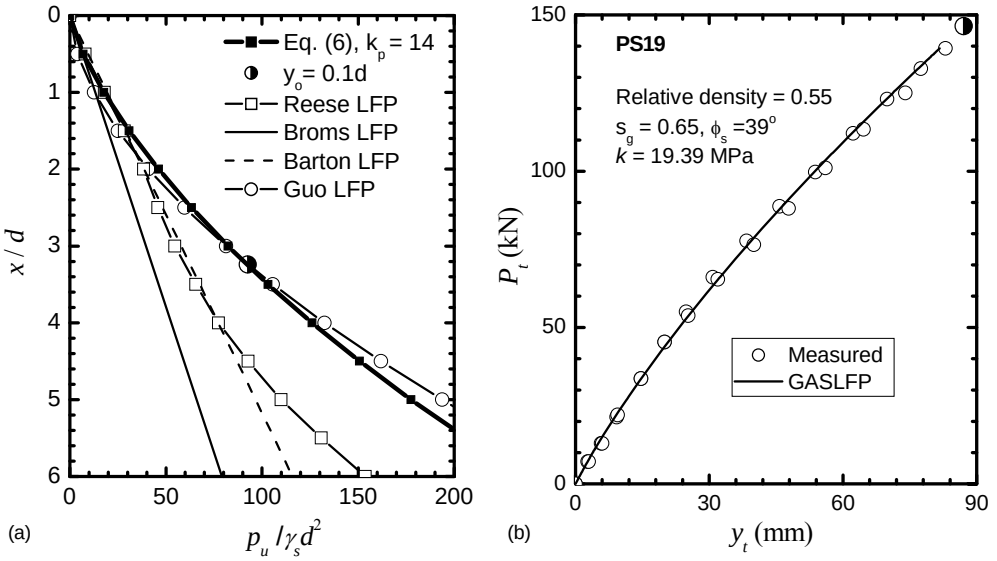

Figure 15: Predicted vs measured (McVay et al. 1995) responses of pile PS19: (a) p_u profiles, and (b) P_t-y_t curves

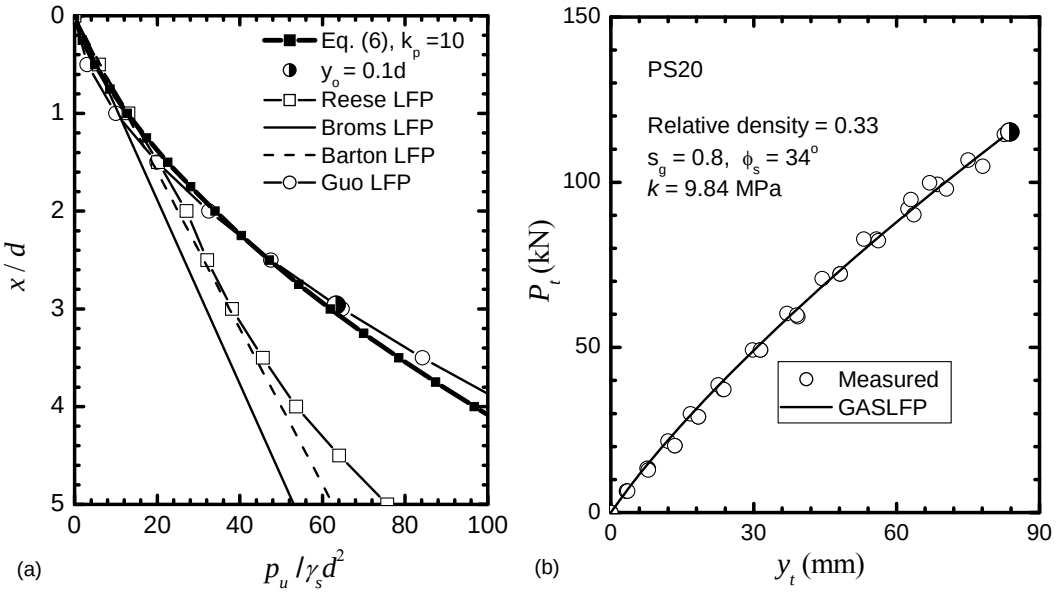

Figure 16: Predicted vs measured (McVay et al. 1995) responses of pile PS20: (a) p_u profiles, and (b) P_t-y_t curves

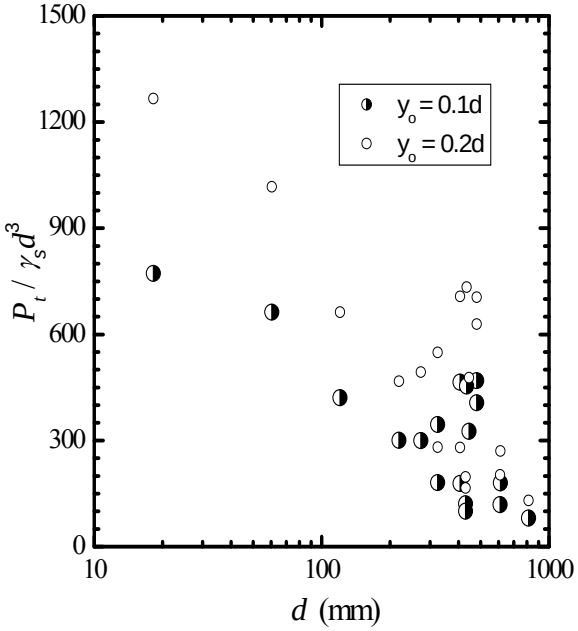

Figure 17: $P_t/\gamma_s d^3 \sim d$ relationship (20 piles)

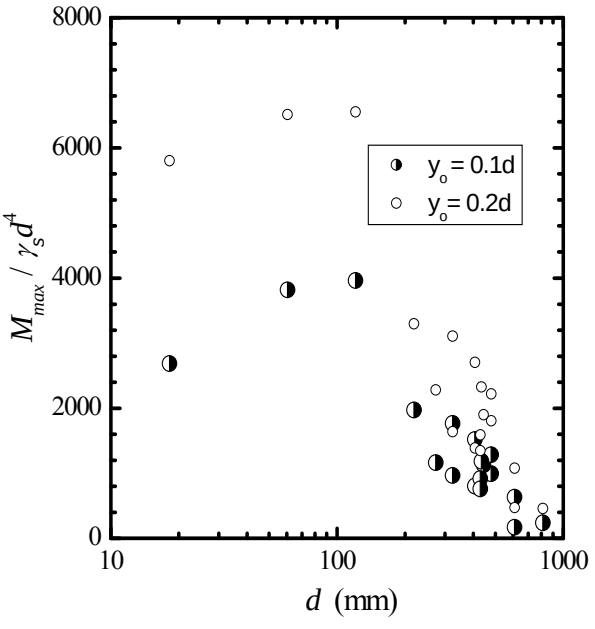

Figure 18: $M_{max}/\gamma_s d^4 \sim d$ relationship (20 piles)